

Reduced Order Optimal Control of the Convective FitzHugh-Nagumo Equation

Bülent Karasözen^a, Tuğba Küçükseyhan^b, Murat Uzunca^{c,*}

^a*Institute of Applied Mathematics & Department of Mathematics, Middle East Technical University, 06800 Ankara, Turkey*

^b*Department of Mathematics, Balıkesir University, 10145 Balıkesir, Turkey*

^c*Department of Industrial Engineering, University of Turkish Aeronautical Association, Ankara*

Abstract

We compare three different model order reduction techniques with Galerkin projection: the proper orthogonal decomposition (POD), POD-DEIM (discrete empirical interpolation) and POD-DMD (dynamic mode decomposition) for solving optimal control problems governed by the convective FitzHugh-Nagumo (FHN) equation. The convective FHN equation consists of the semilinear activator and the linear inhibitor equation, modelling blood coagulation in moving excitable media. The POD and POD-DEIM reduced optimal control problems are non-convex due to the nonlinear activator equation. DMD is an equation-free, data-driven method which extracts dynamically relevant information content without explicitly knowing the dynamical operator. We use DMD as an alternative method to DEIM in order to approximate the nonlinear term in the convective FHN equation. Applying the POD-DMD Galerkin projection gives rise to a linear system of equations for the activator, and the optimal control problem becomes convex. We compare the accuracy and CPU times of three reduced order methods (ROM) with respect to the full order discontinuous Galerkin finite element solutions for convection dominated wave type solutions with terminal controls. Numerical results show that POD is the most accurate whereas POD-DMD is the fastest.

Keywords: FitzHugh-Nagumo equation; optimal control; discontinuous Galerkin method; proper orthogonal decomposition; discrete empirical interpolation; dynamic mode decomposition.

*Corresponding author

Email addresses: bulent@metu.edu.tr (Bülent Karasözen),
guney.tugba@metu.edu.tr (Tuğba Küçükseyhan), muzunca@thk.edu.tr (Murat Uzunca)

1. Introduction

Optimal control of nonlinear partial differential equations (PDEs) with wave type solutions became an active research field in the recent years. We can mention the control of Schlögl or Nagumo equation with spiral waves [1], of classical FitzHugh-Nagumo equation with spiral and travelling waves [2, 3, 4], of lambda-omega systems with spiral waves [5]. In this paper we investigate reduced order optimal control of the convective FitzHugh-Nagumo (FHN) equation modelling blood coagulation and bioreactors [6, 7]. The FHN equation is the simplest and most widely used model for describing the complex spatio-temporal behavior of travelling waves in excited media. In contrast to the classical FHN equation [8, 9] with a semi-linear PDE and with a linear ordinary differential equation (ODE), the convective FHN equation consists of a semi-linear PDE with monotone cubic nonlinear term for the activator and a linear PDE for the inhibitor, modelling excitable systems in moving media.

The discretization of the optimal control problems (OCPs) with PDE constraints in space and time results high dimensional systems. Here, we use symmetric interior penalty Galerkin (SIPG) method for space discretization [10]. The discontinuous Galerkin (dG) methods are more stable for convection dominated problems than the continuous finite element methods and they do not require the stabilization terms like the streamline upwind/Petrov-Galerkin method (SUPG). The dG methods have several advantages compared to other numerical techniques such as finite volume and finite element methods; the trial and test spaces can be easily constructed, inhomogeneous boundary conditions and curved boundaries can be handled easily. The dG methods were successfully applied to linear steady state, time dependent and semi-linear optimal control problems with convection-diffusion-reaction equations [11, 12, 13]; to the semi-linear steady state OCPs [14]. There are two approaches for solving OCPs with PDE constraints. The first one is the discretize-then-optimize approach, where the objective function is discretized and the discrete Lagrangian is built, and then the optimality conditions are imposed in the discrete setting. The second one is the optimize-then-discretize approach, where the Lagrangian is built for the infinite dimensional problem and then the first order optimality conditions are discretized. There is no preferred approach [15, 16], here we follow the optimize-then-discretize approach using the SIPG discretization in space and the backward Euler method in time. We employ the projected nonlinear conjugate gradient (CG) method [17] for solving the

nonlinear discrete optimization problem.

Due to the computational cost of large scale PDE constrained OCPs, we consider reduced order optimal control of the convective FHN equation. For a recent overview about the reduced order methods for OCPs we refer to [15, 16]. The reduced order OCPs are solved usually applying the Galerkin projection based on the proper orthogonal decomposition (POD) using the snapshots of the discretized state equation. Despite its heuristic nature, the POD is currently the most popular and successful model reduction technique for solving linear and nonlinear OCPs. The POD basis functions contain information from the solutions of the dynamical system at pre-specified time-instances, so-called snapshots, which inhibit the main and relevant physical properties of the state system. Increasing the number of the POD basis functions leads to more accurate reduced order or suboptimal controls, which can be considered as a compensate for the lack of a priori analysis of the POD. Reduced order methods (ROMs) using the POD-Galerkin projection for OCPs with linear PDE constraints are investigated in [18, 19, 20] and with semi-linear PDE constraints in [21, 22, 23], where a priori and a posteriori error estimates are derived. Although the POD method is used frequently for nonlinear PDEs, the evaluation of the nonlinear term still depends on the dimension of the full order model (FOM), i.e., high dimensional finite element discretized model. The empirical interpolation method (EIM) [24] and the discrete empirical interpolation (DEIM) method [25] are used to reduce the computational cost for evaluation of the nonlinear terms. More recently, as an alternative to the DEIM, the dynamic mode decomposition (DMD) [26] is used to approximate the nonlinear terms of the PDEs. DMD was first introduced by Schmid [27], Rowley [28] and it is based on the approximation of the linear infinite dimensional Koopman operator [29]. For an overview of the DMD and various applications we refer the reader to the recent monograph [30].

In this paper, we compare three different reduced order approaches the proper orthogonal decomposition (POD), POD with the discrete empirical interpolation (DMD) and POD with dynamic mode decomposition (DMD) by comparing the accuracy and computational time of the reduced order suboptimal solutions. To our best knowledge, reduced order OCPs using POD-DMD are not yet investigated in the literature. When dealing with model order reduction, it is important to have a trade-off between the computational cost and accuracy of the reduced solutions. Among these three methods, POD-DMD is the fastest, because after collecting snapshots, the nonlinearity disappear and the reduced model becomes a coupled system linear system ODEs. Also the reduced nonconvex optimization problem for POD and POD-DEIM, becomes convex for POD-DMD. The

POD is the most accurate but, the slowest. The POD-DMD is less accurate than the POD, but fastest. The success of POD depends on the type of the problem. The reduced or suboptimal control of semilinear PDEs [21] and convection dominated problems with travelling wave solutions require greater number of POD basis functions [31], which is also confirmed by numerical results in Section 5.

The outline of this paper is as follows. In Section 2 the OCP with pointwise box constraints governed by convective FHN equation is described. The first order optimality conditions are derived in Section 3 with the fully discrete optimal control system in space and time are recalled. In Section 4, reduced order models POD, POD-DEIM and POD-DMD are derived for the OCP governed by the convective FHN equation. In Section 5 we compare the three reduced order techniques with respect to accuracy and computational time for a test problem with terminal controls. The paper ends with some conclusions.

2. Optimal control problem

We consider the following OCP

$$\begin{aligned} \min_{u \in \mathcal{U}_{ad}} J(y, u) = & \frac{1}{2} \int_{\Omega} (y(x, T) - y_T(x))^2 dx + \frac{1}{2} \int_{\Omega} (z(x, T) - z_T(x))^2 dx \\ & + \frac{\lambda}{2} \int_0^T \int_{\Omega} u(x, t)^2 dx dt, \end{aligned} \quad (1)$$

subject to the convective FHN equation

$$y_t(x, t) - D_1 \Delta y(x, t) + \mathbf{V} \cdot \nabla y(x, t) + g(y(x, t)) + z(x, t) = u(x, t) \quad \text{in } Q, \quad (2a)$$

$$z_t(x, t) - D_2 \Delta z(x, t) + \mathbf{V} \cdot \nabla z(x, t) + \varepsilon(z(x, t) - c_3 y(x, t)) = 0 \quad \text{in } Q, \quad (2b)$$

with the Neumann and Dirichlet boundary conditions

$$\begin{aligned} \partial_n y(x, t) = 0, \quad \partial_n z(x, t) = 0 & \quad \text{on } \Sigma^N, \\ y(x, t) = y_D(x, t), \quad z(x, t) = z_D(x, t) & \quad \text{on } \Sigma^D, \end{aligned}$$

and with the initial conditions

$$y(x, 0) = y_0(x), \quad z(x, 0) = z_0(x) \quad \text{in } \Omega,$$

and subject to the pointwise box constraints

$$u \in \mathcal{U}_{ad} := \{u \in L^\infty(Q) : u_l \leq u(x, t) \leq u_r \text{ for a.e } (x, t) \in Q\} \quad (4)$$

with the real numbers $u_l \leq u_r$.

Here $T > 0$ denotes the final time and Q denotes the time space cylinder $Q := \Omega \times (0, T]$, where $\Omega = (0, L) \times (0, H)$ is a bounded, Lipschitz domain in \mathbb{R}^2 . The lateral surface is denoted by $\Sigma = \partial\Omega \times (0, T]$. We use the notation $\Sigma^D := \Gamma_D \times (0, T]$ and $\Sigma^N := \Gamma_N \times (0, T]$, where $\Gamma_D = \{x_1 = 0, L, 0 < x_2 < H\}$ and $\Gamma_N = \{0 < x_1 < L, x_2 = 0, H\}$ are Dirichlet and Neumann boundaries, respectively. We denote the outward unit normal vector and the associated outward normal derivative on $\partial\Omega$ by \mathbf{n} and ∂_n , respectively. The diffusion coefficients are denoted by D_1 and D_2 . The parameters c_3 and ε are real constants. Further, the function $g(y)$ denotes the cubic polynomial nonlinearity

$$g(y) = c_1 y(y - c_2)(y - 1) \quad (5)$$

with the non-negative real numbers $c_i, i = 1, 2$, which is monostable for $0 < c_1 < 20$ and $c_2 = 0.02$ [6] in contrast to the bistable cubic nonlinearity for the Schlögl equation [1], the classical FHN equation [2], and the diffusive FHN equation [32]. The velocity field denoted by $\mathbf{V} = (V_{x_1}, V_{x_2})$ which is given along the x_1 -direction with a parabolic profile

$$V_{x_1}(x_2) = ax_2(H - x_2), \quad V_{max} = \frac{1}{4}aH^2, \quad a > 0, \quad V_{x_2} = 0, \quad (6)$$

where V_{max} denotes the maximum wave speed of the velocity field. Moreover, the velocity field is divergence free, i.e., $\text{div } \mathbf{V} = 0$.

The aim of the optimal control problem (2) is to minimize the cost functional $J(y, u)$ to ensure that the state variables, activator y and the inhibitor z are as close as possible in the L_2 norm to the desired states $y_T(x), z_T(x)$ at the final time T . The activator y is to be controlled by u , while the inhibitor z has only some auxiliary character with respect to the control as for the classical FHN equation [2, 3, 4], because only controlling the activator seems to be experimentally feasible [33]. In (2), $\lambda > 0$ denotes the penalization or the Tikhonov regularization parameter.

Mathematical modeling of an excitable medium requires at least two equations, one of them is the activator and the other is the inhibitor equation. In blood coagulation process, the activator variable y describes the concentrations of thrombin the excitation itself, and another describes the inhibition of this excitation and recovery of the medium variables, z activated factor XI [7]. The complex process of coagulation consists of cascadic enzymatic reactions and feedback loops, differentiated into three stages, initiation (localized at the vascular damage site); propagation, or spatial expansion of coagulation wave into the vessel; termination of the biochemical reactions and clot enlargement stoppage [34]. These ultimately catalyze fibrinogen conversion into fibrin, which polymerizes to form a

clot. These reactions allows autocatalytic thrombin generation far from the damage site. The most important property of blood coagulation process is the formation of autowaves with the velocity independent of the initial conditions [6, 7, 34]. The flow propagates within the impermeable channel walls (Neumann boundary conditions). Different type of standing and triggering waves occur depending on the constants of the convective FHN equation [6]. The waves became more curved when the flow velocity V_{max} increases. For a detailed discussion of the complex spatio-temporal wave phenomena occurring in the uncontrolled convective FHN equation we refer the reader to [6, 35].

The waves are initiated at $t = 0$ inside a narrow rectangle $\{x_a \leq x \leq x_b, 0 \leq x_2 \leq H\}$ as:

$$y_0(x, t) = \begin{cases} 0.1, & \text{if } 0 \leq x_1 \leq 0.1, \\ 0, & \text{otherwise,} \end{cases} \quad z_0(x, 0) = 0. \quad (7)$$

This rectangle is also called the initial excitation region, where the interval from x_a to x_b imitates the damaged region of the vessel wall, and setting a fixed thrombin concentration in in mimics the activation process of blood coagulation [6, 7, 34].

3. Optimality system and discretization

We use optimize-then-discretize approach to derive the optimality conditions in the variational form and discretize the full order OCP problem. The weak form of the state equations (2) are given as

$$(y_t, v)_\Omega + D_1 a(y, v) + b(y, v) + (g(y), v)_\Omega + (z, v)_\Omega = (u, v)_\Omega, \quad (8a)$$

$$(y(\cdot, 0), v)_\Omega = (y_0, v)_\Omega, \quad (8b)$$

$$(z_t, v)_\Omega + D_2 a(z, v) + b(z, v) + \varepsilon(z, v)_\Omega - \varepsilon c_3(y, v)_\Omega = 0, \quad (8c)$$

$$(z(\cdot, 0), v)_\Omega = (z_0, v)_\Omega, \quad (8d)$$

where $(\cdot, \cdot)_\Omega$ denotes the L_2 inner product in Ω , and from now, we set $(\cdot, \cdot) := (\cdot, \cdot)_\Omega$ for easy notation. The symmetric bi-linear forms for the diffusive terms are given as $a(y, v) = (\nabla y, \nabla v)$, $a(z, v) = (\nabla z, \nabla v)$, whereas $b(y, v) = (\mathbf{V} \cdot \nabla y, v)$, $b(z, v) = (\mathbf{V} \cdot \nabla z, v)$ denote the non-symmetric bi-linear forms for the convective terms, and $v \in H_1^0(\Omega)$ is a test function.

Here we consider only the first order optimality conditions. We refer to [2, 36] for a discussion of the second order necessary and sufficiency optimality conditions for semilinear parabolic equations. The first-order necessary optimality

conditions for the system (8) are derived using the Lagrangian framework see, e.g., [36, Chapter 1]

$$-(p_t, v) + D_1 a(p, v) - b(p, v) + (g_y p, v) - \varepsilon c_3(q, v) = 0, \quad (9a)$$

$$(p(\cdot, T), v) = (y - y_T, v), \quad (9b)$$

$$-(q_t, v) + D_2 a(q, v) - b(q, v) + \varepsilon(q, v) + (p, v) = 0, \quad (9c)$$

$$(q(\cdot, T), v) = (z - z_T, v), \quad (9d)$$

with the mixed boundary, with the Dirichlet boundary and the terminal time conditions

$$\begin{aligned} D_1 \partial_n \bar{p}(x, t) + (\mathbf{V} \cdot \mathbf{n}) p(x, t) &= 0, & D_2 \partial_n q(x, t) + (\mathbf{V} \cdot \mathbf{n}) q(x, t) &= 0, & \text{on } \Sigma^N, \\ p(x, t) &= 0, & q(x, t) &= 0, & \text{on } \Sigma^D, \\ p(x, T) &= y(x, T) - y_T(x), & q(x, T) &= z(x, T) - z_T(x), & \text{in } \Omega. \end{aligned}$$

We also have, for the optimal solution $(\bar{y}, \bar{p}, \bar{u})$, the following variational inequality

$$\int_0^T \int_{\Omega} (\bar{p}(x, t) + \lambda \bar{u}(x, t)) (u(x, t) - \bar{u}(x, t)) dx dt \geq 0 \quad \forall u \in \mathcal{U}_{ad}. \quad (11)$$

The bi-linear forms for the convection terms $b(p, v)$, $b(q, v)$ in (9) have negative directions, i.e. the adjoints flow in the opposite direction of the states.

3.1. Space discretization of the optimal control problem

In this section we give the space-time discretization of the PCP (2). We first give symmetric interior penalty Galerkin (SIPG) discretization in space for state and adjoint equations. Then, the full discrete form is derived using backward Euler method in time.

We denote the mesh by \mathcal{T}_h which consists of non-overlapping triangular elements K . h_K and h_E denote the diameter of an element K and the length of an edge E , respectively. We use the space of discontinuous piecewise finite element functions to define the discrete test, state and control spaces

$$V_h = \{v \in L^2(\Omega) : v|_K \in \mathbb{P}^p(K) \quad \forall K \in \mathcal{T}_h\}.$$

where $\mathbb{P}^p(K)$ denotes the set of all polynomials on $K \in \{\mathcal{T}_h\}$ of degree at most p . For our numerical examples p is chosen as 1.

We split all the edges E_h into the sets of interior, Dirichlet boundary and Neumann boundary edges, denoted respectively by E_h^0, E_h^D, E_h^N , such that $E_h = E_h^0 \cup E_h^D \cup E_h^N$. Let \mathbf{n} denotes the unit outward normal to $\partial\Omega$. We define the inflow boundary $\Gamma^- = \{x \in \partial\Omega : \mathbf{V} \cdot \mathbf{n}(x) < 0\}$ and the outflow boundary $\Gamma^+ = \partial\Omega \setminus \Gamma^-$. The inflow and outflow boundaries of an element $K \in \mathcal{T}_h$ are defined by

$$\partial K^- = \{x \in \partial K : \mathbf{V} \cdot \mathbf{n}_K(x) < 0\}, \quad \partial K^+ = \partial K \setminus \partial K^-,$$

where \mathbf{n}_K is the unit normal vector on the boundary ∂K of an element K .

Let the edge E be a common edge for two elements K and K^e . For a scalar function $v \in V_h$, there are two traces of v along E , denoted by $v|_E$ from interior of K and $v^e|_E$ from interior of K^e . Then, the jump and average of v across the edge E are defined by:

$$[[v]] = v|_E \mathbf{n}_K + v^e|_E \mathbf{n}_{K^e}, \quad \{\{v\}\} = \frac{1}{2}(v|_E + v^e|_E).$$

Similarly, for a vector field ∇v , the jump and average across an edge E are given by

$$[[\nabla v]] = \nabla v|_E \cdot \mathbf{n}_K + \nabla v^e|_E \cdot \mathbf{n}_{K^e}, \quad \{\{\nabla v\}\} = \frac{1}{2}(\nabla v|_E + \nabla v^e|_E).$$

For a boundary edge $E \in K \cap \partial\Omega$, we set $[[v]] = v|_E \mathbf{n}$ and $\{\{\nabla v\}\} = v|_E$. Then, SIPG discretized forms of the state equation (2) and of the adjoint read as: $\forall v_h \in V_h$ and a.e. $t \in (0, T]$

$$\left(\frac{dy_h}{dt}, v \right) + D_1 a_h(y_h, w) + b_h(y_h, w) + g(y_h, w) + (z_h, w) = \ell_{h,y}(w) + (u_h, w), \quad (12a)$$

$$(y_h(\cdot, 0), w) = (y_0, w),$$

$$\left(\frac{dz_h}{dt}, v \right) + D_2 a_h(z_h, w) + b_h(z_h, w) + \varepsilon(z_h, w) - \varepsilon c_3(y_h, w) = \ell_{h,z}(w), \quad (12b)$$

$$(z_h(\cdot, 0), w) = (z_0, w),$$

$$\left(-\frac{dp_h}{dt}, w \right) + D_1 a_{h,p}(p_h, w) - b_h(p_h, w) + g_y(p_h, w) - \varepsilon c_3(q_h, w) = 0, \quad (13a)$$

$$(p_h(\cdot, T), w) = ((y_h(\cdot, T) - y_T(x)), w),$$

$$\left(-\frac{dq_h}{dt}, w \right) + D_2 a_{h,q}(q_h, w) - b_h(q_h, w) + \varepsilon(q_h, w) + (p_h, w) = 0, \quad (13b)$$

$$(q_h(\cdot, T), w) = ((z_h(\cdot, T) - z_T(x)), w),$$

where the bi-linear terms are defined for $\eta = y, z, i = 1, 2$ and $\forall v, w \in V_h$

$$\begin{aligned}
a_h(v, w) &= \sum_{K \in \mathcal{T}_h} \int_K \nabla v \cdot \nabla w \, dx \\
&\quad - \sum_{E \in \mathcal{E}_h^0 \cup \mathcal{E}_h^D} \int_E \left(\{\{\nabla v\}\} \cdot \llbracket w \rrbracket + \{\{\nabla w\}\} \cdot \llbracket v \rrbracket \right) ds \\
&\quad + \sum_{E \in \mathcal{E}_h^0 \cup \mathcal{E}_h^D} \frac{\gamma}{h_E} \int_E \llbracket v \rrbracket \cdot \llbracket w \rrbracket \, ds, \tag{14a}
\end{aligned}$$

$$\begin{aligned}
b_h(v, w) &= \sum_{K \in \mathcal{T}_h} \int_K \mathbf{v} \cdot \nabla v w \, dx \\
&\quad + \sum_{K \in \mathcal{T}_h} \int_{\partial K^- \setminus \partial \Omega} \mathbf{v} \cdot \mathbf{n} (v^e - v) w \, ds - \sum_{K \in \mathcal{T}_h} \int_{\partial K^- \cap \Gamma^-} \mathbf{v} \cdot \mathbf{n} v w \, ds, \tag{14b}
\end{aligned}$$

$$\begin{aligned}
\ell_{h,i}(w) &= \sum_{E \in \mathcal{E}_h^D} \int_E \eta_D \left(\frac{\gamma D_i}{h_E} \mathbf{n} \cdot \llbracket w \rrbracket - \{\{D_i \nabla w\}\} \right) ds \\
&\quad - \sum_{K \in \mathcal{T}_h} \int_{\partial K^- \cap \Gamma^-} \mathbf{v} \cdot \mathbf{n} \eta_D v \, ds \tag{14c}
\end{aligned}$$

$$g(v, w) = \sum_{K \in \mathcal{T}_h} \int_K g(v) w \, dx, \quad g_y(v, w) = \sum_{K \in \mathcal{T}_h} \int_K g_y(y) v w \, dx, \tag{14d}$$

where the parameter γ is called the penalty parameter and it should be sufficiently large to ensure the stability of the DG discretization [10] with a lower bound depending only on the polynomial degree. The bi-linear forms $a_{h,p}$ and $a_{h,q}$ for the adjoint are similar to the ones for states, a_h , but contain the contribution of the mixed boundary conditions, i.e., they includes additionally, respectively, the terms

$$\sum_{E \in \mathcal{E}_h^N} \int_E (\mathbf{v} \cdot \mathbf{n}) p_h w \, ds \quad \text{and} \quad \sum_{E \in \mathcal{E}_h^N} \int_E (\mathbf{v} \cdot \mathbf{n}) q_h w \, ds.$$

The solutions of (12) are given by

$$y_h(t) = \sum_{i=1}^{n_e} \sum_{j=1}^{n_p} y_j^i \phi_j^i, \quad z_h(t) = \sum_{i=1}^{n_e} \sum_{j=1}^{n_p} z_j^i \phi_j^i, \quad \text{and} \quad u_h(t) = \sum_{i=1}^{n_e} \sum_{j=1}^{n_p} u_j^i \phi_j^i, \tag{15}$$

where n_e denotes the number of (triangular) elements, n_p is the local dimension of each element, and ϕ_j^i is the j -th finite element basis function defined on the i -th triangle. Setting the dG degrees of freedom $N := n_e \times n_p$, the corresponding unknown coefficients

$$\begin{aligned}\vec{y} &= (y_1^1, \dots, y_{n_p}^1, \dots, y_1^{n_e}, \dots, y_{n_p}^{n_e}) \in \mathbb{R}^N, \\ \vec{z} &= (z_1^1, \dots, z_{n_p}^1, \dots, z_1^{n_e}, \dots, z_{n_p}^{n_e}) \in \mathbb{R}^N, \\ \vec{u} &= (u_1^1, \dots, u_{n_p}^1, \dots, u_1^{n_e}, \dots, u_{n_p}^{n_e}) \in \mathbb{R}^N.\end{aligned}$$

Then, the SIPG semi-discretized system of state equations (12) lead to the ODEs of the form

$$\mathbf{M} \frac{d\vec{y}}{dt} + D_1 \mathbf{S} \vec{y} + \mathbf{B} \vec{y} + \mathbf{g}(\vec{y}) + \mathbf{M} \vec{z} = \ell_y + \mathbf{M} \vec{u}, \quad (16a)$$

$$\mathbf{M} \frac{d\vec{z}}{dt} + D_2 \mathbf{S} \vec{z} + \mathbf{B} \vec{z} + \varepsilon \mathbf{M} \vec{z} - \varepsilon c_3 \mathbf{M} \vec{y} = \ell_z, \quad (16b)$$

where \mathbf{M} is the mass matrix, \mathbf{S} and \mathbf{B} are symmetric and non-symmetric parts of the stiffness matrices corresponding to the diffusive and convective terms, $\mathbf{g}(\vec{y})$ is the nonlinear vector, and ℓ_y and ℓ_z are the vectors corresponding to the linear forms $\ell_{h,y}$ and $\ell_{h,z}$, respectively. By a similar setting, the SIPG semi-discretized system of the adjoint equations (13) are given as

$$-\mathbf{M} \frac{d\vec{p}}{dt} + D_1 \mathbf{S} \vec{p} - \mathbf{B} \vec{p} + \mathbf{R}_g \vec{p} - \varepsilon c_3 \mathbf{M} \vec{q} = 0, \quad (17a)$$

$$-\mathbf{M} \frac{d\vec{q}}{dt} + D_2 \mathbf{S} \vec{q} - \mathbf{B} \vec{q} + \varepsilon \mathbf{M} \vec{q} + \mathbf{M} \vec{p} = 0, \quad (17b)$$

where the matrix \mathbf{R}_g is related to the form $g_y(p_h, w)$ which is defined in (14).

3.2. Full discrete optimality system

We consider the uniform partition of time interval $[0, T]$ as $0 = t_0 < t_1 < \dots < t_{N_T} = T$, with the time step-size $\Delta t = T/N$. As the time integrator, we use the backward Euler method. The application of the backward Euler method to (16) and (17) leads to the full discrete system

$$\frac{1}{\Delta t} \mathbf{M} (\vec{y}_n - \vec{y}_{n-1}) + D_1 \mathbf{S} \vec{y}_n + \mathbf{B} \vec{y}_n + \mathbf{g}(\vec{y}_n) + \mathbf{M} \vec{z}_n = \ell_y^n + \mathbf{M} \vec{u}_n, \quad (18a)$$

$$\frac{1}{\Delta t} \mathbf{M} (\vec{z}_n - \vec{z}_{n-1}) + D_2 \mathbf{S} \vec{z}_n + \mathbf{B} \vec{z}_n + \varepsilon \mathbf{M} \vec{z}_n - \varepsilon c_3 \mathbf{M} \vec{y}_n = \ell_z^n, \quad (18b)$$

$$(\mathbf{M} \vec{y}_0)_i = (y_0, \phi_i), \quad \mathbf{M} (\vec{z}_0)_i = (z_0, \phi_i), \quad i = 1, 2, \dots, N, \quad (18c)$$

for $n = 1, 2, \dots, N_T$, and

$$\frac{1}{\Delta t} \mathbf{M}(\vec{p}_{n-1} - \vec{p}_n) + D_1 \mathbf{S} \vec{p}_{n-1} - \mathbf{B} \vec{p}_{n-1} + \mathbf{g}_y(\vec{y}_n) \vec{p}_{n-1} - \varepsilon c_3 \mathbf{M} \vec{q}_{n-1} = 0, \quad (19a)$$

$$\frac{1}{\Delta t} \mathbf{M}(\vec{q}_{n-1} - \vec{q}_n) + D_2 \mathbf{S} \vec{q}_{n-1} - \mathbf{B} \vec{q}_{n-1} + \varepsilon \mathbf{M} \vec{q}_{n-1} + \mathbf{M} \vec{p}_{n-1} = 0, \quad (19b)$$

$$(\mathbf{M} \vec{p}_{N_T})_i = (\mathbf{M} \vec{y}_{N_T})_i - (y_T, \phi_i), \quad (\mathbf{M} \vec{q}_{N_T})_i = (\mathbf{M} \vec{z}_{N_T})_i - (z_T, \phi_i) \quad i = 1, 2, \dots, N, \quad (19c)$$

for $n = N_T, \dots, 2, 1$. Although the full discrete state equation (18) is solved forward in time, the full discrete adjoint equation (19) is solved backward in time.

There exists several optimization algorithms for solving the OCPs governed by semi-linear equations. We have used in this paper the projected nonlinear conjugate gradient (CG) method [17], which was applied to the Schlögl and FHN equations [1, 2, 3, 4] and to the convective FHN equation [32]. The details of the implementation of projected nonlinear CG algorithm can be found in these papers.

4. Reduced order optimal control

In this section we give the POD, POD-DEIM and POD-DMD Galerkin discretization of the full discrete optimality system (18)-(19). The adjoint states are approximated by their own POD basis. We have used the same POD basis generated by the snapshots of states y and z for construction of the reduced adjoint equations motivated by the error analysis in [16]. Using the same POD basis functions for the states and adjoints might be not the best option. But, the construction different reduced stiffness, convection and mass matrices using the POD basis from the snapshots of the adjoints does not improve the suboptimal solutions much [21] and requires more computational work. The POD was applied for distributed and boundary optimal control of the classical FHN equation without using the DEIM in [21, 37]. We want to mention the snapshots for the POD and DMD are corresponding to the coefficient vectors of the dG solutions in contrast to the continuous finite elements where the snapshots are the FEM solutions.

4.1. The POD Galerkin discretization

The reduced-order system for the state equations (18) of lower dimension k is formed by the Galerkin projections of the equations onto k -dimensional subspaces

$$V_{y,h}^r = \text{span}\{\psi_{y,1}, \dots, \psi_{y,k}\} \subset V_h, \quad V_{z,h}^r = \text{span}\{\psi_{z,1}, \dots, \psi_{z,k}\} \subset V_h,$$

resulting in lower dimensional reduced solutions of the coefficient vectors of the state equations

$$\bar{\mathbf{y}}(t) \approx \bar{\mathbf{y}}_r(t) = \sum_{i=1}^k (\bar{\mathbf{y}}_r)_i(t) \boldsymbol{\psi}_{y,i}, \quad \bar{\mathbf{z}}(t) \approx \bar{\mathbf{z}}_r(t) = \sum_{i=1}^k (\bar{\mathbf{z}}_r)_i(t) \boldsymbol{\psi}_{z,i}, \quad (20)$$

where $\bar{\mathbf{y}}_r(t) = ((\bar{\mathbf{y}}_r)_1(t), \dots, (\bar{\mathbf{y}}_r)_k(t))^T$ and $\bar{\mathbf{z}}_r(t) = ((\bar{\mathbf{z}}_r)_1(t), \dots, (\bar{\mathbf{z}}_r)_k(t))^T$ are the solutions of the reduced state system, and $\{\boldsymbol{\psi}_{y,i}\}_{i=1}^k$ and $\{\boldsymbol{\psi}_{z,i}\}_{i=1}^k$ are the orthogonal (in L^2 -sense) reduced basis functions. Belonging to the space V_h , the reduced basis functions are linear combination of the dG functions $\{\phi_j\}_{j=1}^N$, given by

$$\boldsymbol{\psi}_{y,i} = \sum_{j=1}^N \Psi_{y,j,i} \phi_j(x), \quad \boldsymbol{\psi}_{z,i} = \sum_{j=1}^m \Psi_{z,j,i} \phi_j(x), \quad i = 1, \dots, k. \quad (21)$$

Then, using the column vectors

$$\bar{\boldsymbol{\Psi}}_{y,i} = (\Psi_{y,1,i}, \dots, \Psi_{y,m,i})^T, \quad \bar{\boldsymbol{\Psi}}_{z,i} = (\Psi_{z,1,i}, \dots, \Psi_{z,m,i})^T, \quad i = 1, \dots, k,$$

we construct the following matrices

$$\boldsymbol{\Psi}_y := [\bar{\boldsymbol{\Psi}}_{y,1}, \dots, \bar{\boldsymbol{\Psi}}_{y,k}], \quad \text{and} \quad \boldsymbol{\Psi}_z := [\bar{\boldsymbol{\Psi}}_{z,1}, \dots, \bar{\boldsymbol{\Psi}}_{z,k}]. \quad (22)$$

Using the POD, the M-orthogonal reduced modes $\{\boldsymbol{\Psi}_{y,i}\}$ and $\{\boldsymbol{\Psi}_{z,i}\}$, $i = 1, 2, \dots, k$, are computed [32, 38]. The snapshot matrices are given as $\mathcal{Y} = [\mathbf{y}^1, \dots, \mathbf{y}^J]$ and $\mathcal{Z} = [\mathbf{z}^1, \dots, \mathbf{z}^J]$ in $\mathbb{R}^{N \times J}$, where the columns of the snapshot matrices are the vectors of the discrete solutions $\{\bar{\mathbf{y}}_i\}_{i=1}^J$ and $\{\bar{\mathbf{z}}_i\}_{i=1}^J$, respectively, of the full order model (FOM) (18) at the time instances t_i , $i = 0, 1, \dots, J$. Then, for $w \in \{y, z\}$, the L^2 -orthogonal reduced basis functions $\{\boldsymbol{\psi}_{w,i}\}$, $i = 1, 2, \dots, k$, are given by the solution of the following minimization problem

$$\min_{\boldsymbol{\psi}_{w,1}, \dots, \boldsymbol{\psi}_{w,k}} \frac{1}{J} \sum_{j=1}^J \left\| \mathbf{w}^j - \sum_{i=1}^k (\mathbf{w}^j, \boldsymbol{\psi}_{w,i})_{L^2(\Omega)} \boldsymbol{\psi}_{w,i} \right\|_{L^2(\Omega)}^2$$

subject to $(\boldsymbol{\psi}_{w,i}, \boldsymbol{\psi}_{w,j})_{L^2(\Omega)} = \boldsymbol{\Psi}_{w,i}^T \mathbf{M} \boldsymbol{\Psi}_{w,j} = \delta_{ij}$, $1 \leq i, j \leq k$,

where δ_{ij} is the Kronecker delta. The above minimization problem is equivalent to the eigenvalue problems

$$\mathcal{Y} \mathcal{Y}^T \mathbf{M} \boldsymbol{\Psi}_{y,i} = \sigma_{y,i}^2 \boldsymbol{\Psi}_{y,i}, \quad \mathcal{Z} \mathcal{Z}^T \mathbf{M} \boldsymbol{\Psi}_{z,i} = \sigma_{z,i}^2 \boldsymbol{\Psi}_{z,i}, \quad i = 1, 2, \dots, k \quad (23)$$

for the coefficient vectors $\Psi_{y,:i}$ and $\Psi_{z,:i}$ of the reduced basis functions $\psi_{y,i}$ and $\psi_{z,i}$, respectively. Setting $\widehat{\mathcal{Y}} = R\mathcal{Y}$ and $\widehat{\mathcal{Z}} = R\mathcal{Z}$ (R^T with the Cholesky factorization of the mass matrix \mathbf{M}), we obtain the equivalent formulation of (23) as

$$\widehat{\mathcal{Y}}\widehat{\mathcal{Y}}^T\widehat{\Psi}_{y,:i} = \sigma_{y,i}^2\widehat{\Psi}_{y,:i}, \quad \widehat{\mathcal{Z}}\widehat{\mathcal{Z}}^T\widehat{\Psi}_{z,:i} = \sigma_{z,i}^2\widehat{\Psi}_{z,:i}, \quad i = 1, 2, \dots, k \quad (24)$$

where $\widehat{\Psi}_{\cdot,:i} = R\Psi_{\cdot,:i}$. Because the singular value decomposition (SVD) is more stable than the eigenvalue decomposition, we reformulate the eigenvalue problem as SVD. The solutions $\widehat{\Psi}_{\cdot,:i}$ of (24) are obtained as the first k left singular vectors $\widehat{\Psi}_{u,:i} = \zeta_{u,i}$ and $\widehat{\Psi}_{v,:i} = \zeta_{v,i}$ of SVD of the snapshot matrices $\widehat{\mathcal{Y}}$ and $\widehat{\mathcal{Z}}$, respectively, as

$$\widehat{\mathcal{Y}} = \zeta_y \Sigma_y \beta_y^T, \quad \widehat{\mathcal{Z}} = \zeta_z \Sigma_z \beta_z^T,$$

where the diagonal matrices Σ_y and Σ_z contain the singular values $\sigma_{y,i}$ and $\sigma_{z,i}$, respectively. Using $\widehat{\Psi}_{\cdot,:i} = R\Psi_{\cdot,:i}$, the coefficient vectors $\Psi_{\cdot,:i}$ of the reduced basis functions are computed as

$$\Psi_{y,:i} = R^{-1}\widehat{\Psi}_{y,:i}, \quad \Psi_{z,:i} = R^{-1}\widehat{\Psi}_{z,:i}, \quad i = 1, 2, \dots, k.$$

In addition, between the state coefficient vectors \vec{y} and \vec{z} of FOM, and the state coefficient vectors \vec{y}_r and \vec{z}_r of ROM, we have the relation

$$\begin{aligned} \vec{y} &\approx \Psi_y \vec{y}_r, & \vec{z} &\approx \Psi_z \vec{z}_r, \\ \vec{y}_r &\approx \Psi_y^T \mathbf{M} \vec{y}, & \vec{z}_r &\approx \Psi_z^T \mathbf{M} \vec{z}, \end{aligned}$$

from where we can find the initial reduced vector $\vec{w}_r(0)$.

We finally obtain the following reduced optimality system for the states

$$\frac{d}{dt}\vec{y}_r + D_1 \mathbf{S}_y^r \vec{y}_r + \mathbf{B}_y^r \vec{y}_r + \Psi_y^T \mathbf{g}(\Psi_y \vec{y}_r) + \mathbf{M}_{y,z}^r \vec{z}_r = \Psi_y^T \ell_y + \Psi_y^T \mathbf{M} u, \quad (25a)$$

$$\frac{d}{dt}\vec{z}_r + D_2 \mathbf{S}_z^r \vec{z}_r + \mathbf{B}_z^r \vec{z}_r + \varepsilon \mathbf{M}_z^r \vec{z}_r - \varepsilon c_3 \mathbf{M}_{z,y}^r \vec{y}_r = \Psi_z^T \ell_z, \quad (25b)$$

$$\vec{y}_{r,0} = \Psi_y^T \mathbf{M} \vec{y}_0, \quad \vec{z}_{r,0} = \Psi_z^T \mathbf{M} \vec{z}_0. \quad (25c)$$

In a similar way, we obtain the reduced adjoint system

$$-\frac{d}{dt}\vec{p}_r + \mathbf{S}_y^r \vec{p}_r - \mathbf{B}_y^r \vec{p}_r + \mathbf{M}_y^r \mathbf{g}_y(\vec{y}_n) \vec{p}_r - \varepsilon c_3 \mathbf{M}_{y,z} \vec{q}_r = 0, \quad (26a)$$

$$-\frac{d}{dt}\vec{q}_r + \mathbf{S}_z^r \vec{q}_r - \mathbf{B}_z^r \vec{q}_r + \varepsilon \mathbf{M}_z^r \vec{q}_r + \mathbf{M}_{z,y}^r \vec{p}_r = 0, \quad (26b)$$

$$\vec{p}_{r,N_T} = \Psi_y^T \mathbf{M} \vec{p}_{N_T}, \quad \vec{q}_{r,N_T} = \Psi_z^T \mathbf{M} \vec{q}_{N_T}, \quad (26c)$$

with the reduced matrices are computed using only the FEM stiffness \mathbf{S} , convection \mathbf{B} and mass \mathbf{M}

$$\begin{aligned} \mathbf{S}_y^r &= \Psi_y^T \mathbf{S} \Psi_y, & \mathbf{B}_y^r &= \Psi_y^T \mathbf{B} \Psi_y, & \mathbf{S}_z^r &= \Psi_z^T \mathbf{S} \Psi_z, & \mathbf{B}_z^r &= \Psi_z^T \mathbf{B} \Psi_z \\ \mathbf{M}_z^r &= \Psi_z^T \mathbf{M} \Psi_z, & \mathbf{M}_{z,y}^r &= \Psi_z^T \mathbf{M} \Psi_y, & \mathbf{M}_{y,z}^r &= \Psi_y^T \mathbf{M} \Psi_z, & \mathbf{M}_y^r &= \Psi_y^T \mathbf{M} \Psi_y. \end{aligned}$$

The suboptimality systems (25) and (25) are also solved in time by the backward Euler method.

4.2. Discrete empirical interpolation (DEIM)

In this part, we give the reduced form of state equation (25) resulting from application of the discrete empirical interpolation (DEIM) method [25] to the nonlinear term $\mathbf{g}_y(\Psi_y \vec{y}_r)$. The DEIM aims to approximate the nonlinear function $\mathbf{g}_y(\Psi_y \vec{y}_r)$ by projecting it onto a subspace of the space generated by the non-linear functions and spanned by a basis of dimension $m \ll N$:

$$\mathbf{g}_y(\Psi_y \vec{y}_r) \approx W s(t) \quad (27)$$

with the corresponding coefficient vector $s(t)$. Since it is overdetermined, we find a projection P s.t. $P = [e_{p_1}, \dots, e_{p_m}] \in \mathbb{R}^{N \times m}$ with e_{p_i} is the i -th column of the identity matrix $I \in \mathbb{R}^{N \times N}$. After similar calculations with the POD, the reduced model for the state equations reads as:

$$\frac{d}{dt} \vec{y}_r + D_1 \mathbf{S}_y^r \vec{y}_r + \mathbf{B}_y^r \vec{y}_r + \mathbf{Q} \mathbf{g}^r(\vec{y}_r) + \mathbf{M}_{y,z}^r \vec{z}_r = \Psi_y^T \boldsymbol{\ell}_y + \Psi_y^T \mathbf{M} u, \quad (28a)$$

$$\frac{d}{dt} \vec{z}_r + D_2 \mathbf{S}_z^r \vec{z}_r + \mathbf{B}_z^r \vec{z}_r + \varepsilon \mathbf{M}_{z,y}^r \vec{z}_r - \varepsilon c_3 \mathbf{M}_{z,y}^r \vec{y}_r = \Psi_z^T \boldsymbol{\ell}_z, \quad (28b)$$

where the matrix $\mathbf{Q} := \Psi_y^T W (P^T W)^{-1}$ is computed once in the off-line stage (finite element discretization), and the reduced nonlinear vector $\mathbf{g}^r(\vec{y}_r) := P^T \mathbf{g}^r(\Psi_y \vec{y}_r)$ requires only $m \ll N$ integral evaluations. When DEIM approximation is not used, it requires N integral evaluations. The computation of the \mathbf{Q} requires $N \times n_p$ integral evaluations without DEIM, but it is only $m \times n_p$ with DEIM approximation.

4.3. Dynamic mode decomposition (DMD)

The dynamic mode decomposition (DMD) extracts dynamically relevant spatio-temporal information content from a numerical or experimental data sets. It is a powerful equation-free, data-driven method to analyze complex systems. Without explicit knowledge of the dynamical system, the DMD algorithm determines

eigenvalues, eigenmodes, and spatial structures for each mode. After building the POD basis functions of rank k , we approximate the nonlinear term $\mathbf{g}(\vec{y})$ in the activator equation (16) following the approach in [26].

We define two snapshot matrices \mathbf{G}, \mathbf{G}' formed by the snapshots of the nonlinearity $\mathbf{g}(\vec{y})$ in (16) at $N_T + 1$ equally spaced time instances

$$\mathbf{G} = [\mathbf{g}(\vec{y}_0), \dots, \mathbf{g}(\vec{y}_{N_T-1})], \quad \mathbf{G}' = [\mathbf{g}(\vec{y}_1), \dots, \mathbf{g}(\vec{y}_{N_T})].$$

According to the Koopman operator theory, there exist a matrix \mathbf{A}_G , such the snapshots matrices satisfy

$$\mathbf{G}' = \mathbf{A}_G \mathbf{G}.$$

The unknown matrix \mathbf{A}_G is given as the solution of the minimization problem

$$\min \|\mathbf{G}' - \mathbf{G} \mathbf{A}_G\|_F^2. \quad (29)$$

$\mathbf{A}_G = \mathbf{G}' \mathbf{G}^\dagger$, where \dagger denotes the Moore-Penrose pseudoinverse. The exact DMD algorithm is given in [39].

Algorithm 1 Exact DMD Algorithm

Given the snapshot matrices \mathbf{G} and \mathbf{G}'
 Compute SVD of \mathbf{G} , $\mathbf{G} = U \Sigma V^*$.
 Define $\tilde{\mathbf{A}}_G = U^* \mathbf{G}' V \Sigma^{-1}$.
 Find eigenvalues and eigenvectors of $\tilde{\mathbf{A}}_G W = W \Lambda$.
 Set DMD modes $\Psi^{\text{DMD}} := \mathbf{G}' V \Sigma^{-1} W$.

After applying the DMD Algorithm 1 to the nonlinear vector $\mathbf{g}(\vec{y})$ in (16), we obtain time dependent DMD approximation as

$$\mathbf{g}^{\text{DMD}}(t) = \sum_{j=1}^k \alpha_j \psi_j^{\text{DMD}}(z) \exp(\omega_j t) = \Psi^{\text{DMD}} \text{diag}(e^{\omega^{\text{DMD}} t}) \alpha \quad (30)$$

where $\Psi^{\text{DMD}} = [\psi_1, \dots, \psi_k]$ are DMD basis functions of rank k of the nonlinear vector \mathbf{g} , $\alpha = [\alpha_1, \dots, \alpha_k]$ is the initial vector $\alpha = (\Psi^{\text{DMD}})^\dagger \mathbf{g}(\vec{y}(t_1))$ and $\omega_j = \log(\lambda_j) / \Delta t$, $j = 1, \dots, k$.

After plugging this term into (25), we obtain the following linear reduced model for the activator state equation:

$$\frac{d}{dt} \vec{y}_r + D_1 \mathbf{S}_y^r \vec{y}_r + \mathbf{B}_y^r \vec{y}_r + \Psi_y^T \mathbf{g}^{\text{DMD}}(t) + \mathbf{M}_{y,z}^r \vec{z}_r = \Psi_y^T \ell_y + \Psi_y^T \mathbf{M} \vec{u}. \quad (31)$$

Although the dimension of the system (31) is the same with (28), the main advantage of the system (31) is that it is linear and the OPC problem becomes a convex one. Because the reduced activator equation linear, we do not need to use Newton method. Therefore the POD-DMD is significantly much faster than POD and POD-DEIM.

5. Numerical results

We consider the optimal control problem with desired state functions defined at the final time $T = 1$. The following parameters and initial condition are used:

$$c_1 = 9, \quad c_2 = 0.02, \quad c_3 = 5, \quad \varepsilon = 0.1, \quad D_1 = D_2 = 1, \quad \lambda = 10^{-3},$$

$$y_0(x, t) = \begin{cases} 1, & \text{if } 2 \leq x_1 \leq 2.2, 0 \leq x_2 \leq H \\ 0, & \text{otherwise,} \end{cases} \quad z_0(x, 0) = 0.$$

The desired states are chosen as

$$y_T(x, T) = y_{\text{nat}}(x, T/2) \quad \text{and} \quad z_T(x, T) = z_{\text{nat}}(x, T/2),$$

where y_{nat} and z_{nat} stand for the uncontrolled solutions of the convective FHN equation. The admissible set of controls is chosen as

$$\mathcal{U}_{ad} := \{u \in L^\infty(Q) : -0.01 \leq u(x, t) \leq 0.01 \text{ for a.e. } (x, t) \in Q\}.$$

We use uniform step size in space $\Delta x_1 = \Delta x_2 = 0.5$ and in time $\Delta t = 0.05$. Stopping criteria for FOM solutions is $|J_{old} - J|/|J_{old}| \leq 1e-3$.

The POD basis functions are determined according to the relative information content (RIC)

$$\varepsilon(k) = \frac{\sum_{i=1}^k \sigma_i^2}{\sum_{i=1}^s \sigma_i^2},$$

which represents the energy captured by the first k POD modes over all s POD modes, s is the rank of snapshot matrix, and σ_i is the corresponding singular value of i -th mode. In the following results, k is chosen as $\min_k \varepsilon(k) \geq 99.99\%$.

We consider the convective FHN equations with a fast wave speed $V_{max} = 128$

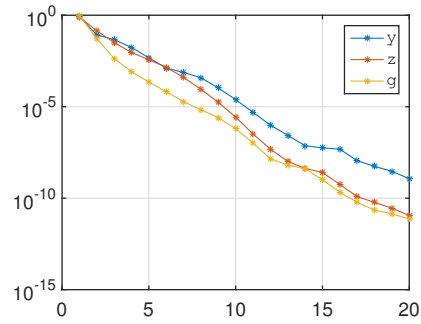


Figure 1: Decay of the singular values for y , z and the nonlinearity g .

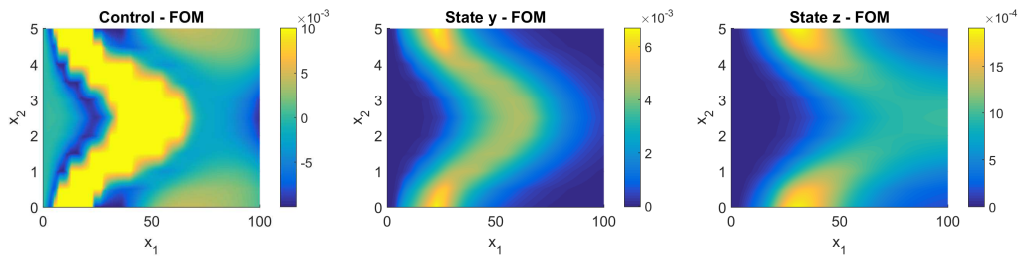


Figure 2: FOM solutions for optimal control u (left) and optimal states y (middle) and z (right) at the final time $T = 1$.

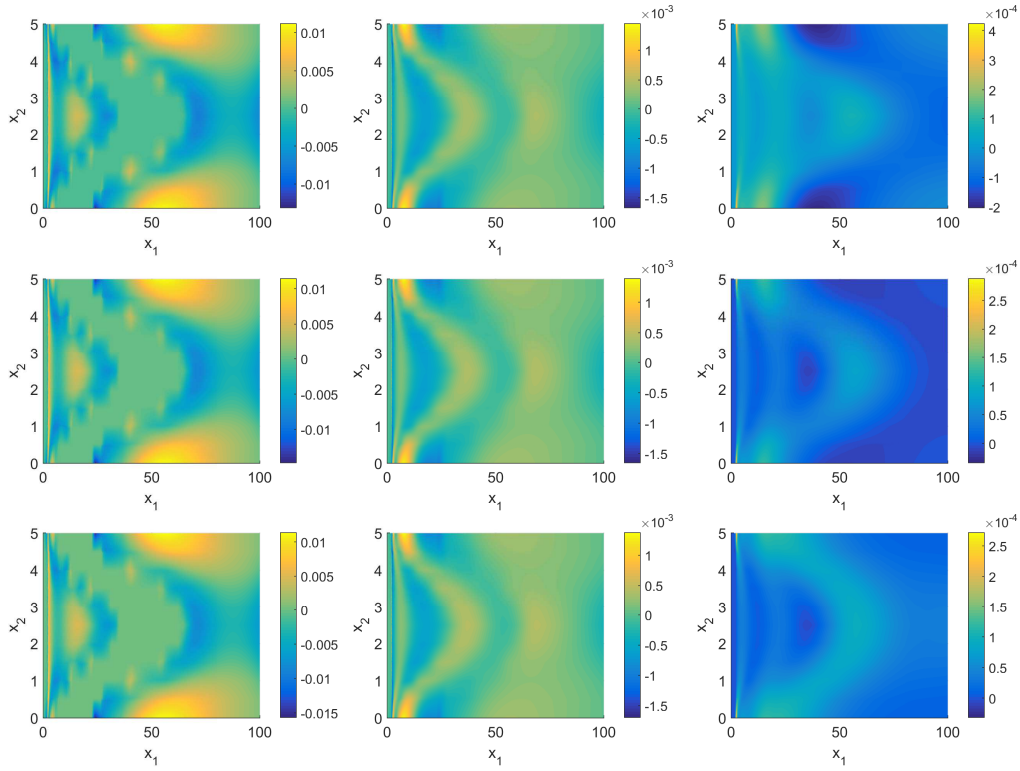


Figure 3: FOM-ROM errors of POD, POD-DEIM and POD-DMD solutions with 8 basis functions (from top to bottom): optimal control u errors (left), associated states y (middle) and z (right) errors at the final time $T = 1$.

	J	# CG iterations	# line searches	#Newton iterations	CPU time	Speedup factor
FOM	1.728e-04	54	205	11.91	6994.80	-
POD	2.140e-04	13	44	9.38	275.80	25.36
POD-DEIM	1.991e-04	14	48	9.64	171.69	40.74
POD-DMD	1.988e-04	14	48	-	50.44	138.69

Table 1: Optimal values of the cost functional J , average number of nonlinear CG iterations, line searches, Newton iterations per time step, and speed-up factors.

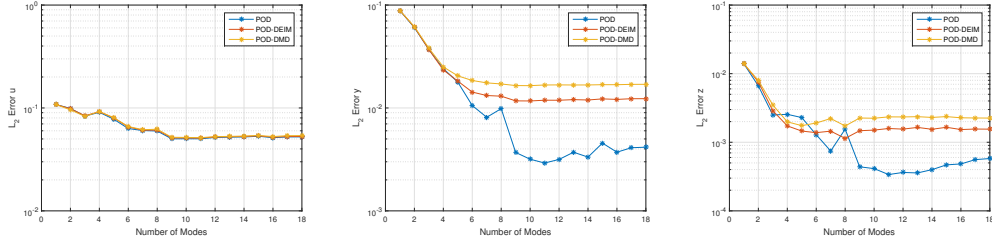


Figure 4: Relative FOM-ROM Frobenius errors: control u (left), states y (middle) and z (right) in the whole domain with increasing number of POD modes.

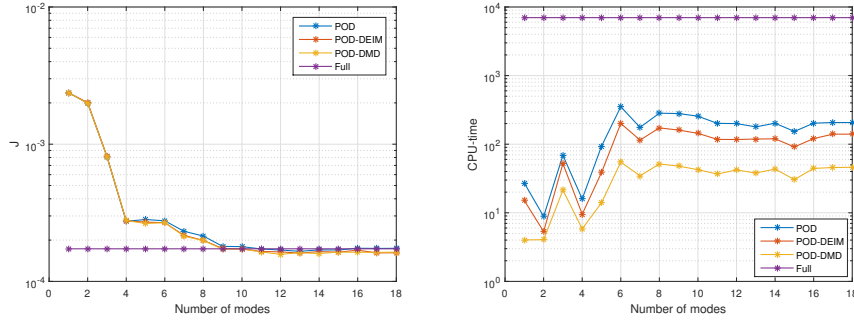


Figure 5: Objective function values (left) and CPU times (right) with increasing number of POD modes.

From Figure 1, it can be seen that the singular values of the snapshot matrices for the states y , z and for the nonlinearity $\mathbf{g}(\vec{y})$ decay almost at the same rate. The energy is captured by $\text{RIC} = 99.99\%$ by $k = 8$ POD modes. The full order solutions in Figure 2 have the same wave type characteristics as in [40]. The ROM errors of the reduced order full order solutions in Figure 3 for the states y , z , and for the control u are at the same order for POD, POD-DEIM and POD-DMD for fixed number of POD basis functions $k = 8$. Because the Galerkin projected POD-DMD system is linear, the resulting OCP problem is convex. Therefore, there is no more Newton iterations in Table 1; instead of nonlinear CG, we use linear CG method. Comparing the speed-up factors (the ratio of the CPU times of the ROM solutions to the CPU times of FOM solutions) in Table 1), the efficiency of POD-DMD solutions clearly visible. The POD reduced sub-optimal solutions are the most accurate, the POD-DEIM and POD-DMD solutions are less accurate, whereas the POD solutions oscillates at lower modes (Figure 4). The objective function J for FOM and ROMS are almost the same with increasing number of

modes in Figure 5, left. The POD requires significantly less CPU time compared to the dG solution. In terms of computational cost the POD-DMD ROM solutions are the fastest (Figure 5, right). At small number of POD modes the CPU times oscillate until $k = 8$ and with increasing number of POD modes they don't change (after $k = 10$). Therefore it is not necessary to use greater number of POD modes considering the CPU times, the accuracy of the ROM solutions and the decrease of the objective function.

6. Conclusions

Among the three ROM techniques the POD is the most accurate as expected. The POD-DEIM and POD-DMD ROM errors are close, but the DMD is the fastest. The POD-DMD is the most efficient due to the fact that we do not have to evaluate the nonlinearity after collecting snapshots. In a further study we plan to compare these ROM techniques for model predictive control and feedback control problems using compressive POD and DMD.

Acknowledgments

This work has been supported by Scientific HR Development Program (ÖYP) of the Turkish Higher Education Council (YÖK).

References

- [1] R. Buchholz, H. Engel, E. Kammann, F. Tröltzsch, On the optimal control of the Schlögl-model, *Computational Optimization and Applications* 56 (1) (2013) 153–185. doi:10.1007/s10589-013-9550-y.
- [2] E. Casas, C. Ryll, F. Tröltzsch, Sparse optimal control of the Schlögl and FitzHugh-Nagumo systems, *Comput. Methods Appl. Math.* 13 (4) (2013) 415–442. doi:10.1515/cmam-2013-0016.
- [3] E. Casas, C. Ryll, F. Tröltzsch, Second order and stability analysis for optimal sparse control of the FitzHugh-Nagumo equation, *SIAM J. Control Optim.* 53 (4) (2015) 2168–2202. doi:10.1137/140978855.
- [4] C. Ryll, J. Löber, S. Martens, H. Engel, F. Tröltzsch, Analytical, optimal, and sparse optimal control of traveling wave solutions to reaction-diffusion

- systems, in: E. Schöll, S. H. L. Klapp, P. Hövel (Eds.), *Control of Self-Organizing Nonlinear Systems*, Springer International Publishing, 2016, pp. 189–210. doi:10.1007/978-3-319-28028-8_10.
- [5] A. Borzi, R. Griesse, Distributed optimal control of lambda–omega systems, *Journal of Numerical Mathematics* 14 (1) (2006) 17–40. doi:10.1163/156939506776382120.
- [6] E. A. Ermakova, E. E. Shnol, M. A. Pantelev, A. A. Butylin, V. Volpert, F. I. Ataullakhanov, On propagation of excitation waves in moving media: The FitzHugh-Nagumo model, *PLoSOne* 4 (2) (2009) E4454. doi:10.1371/journal.pone.0004454.
- [7] E. Ermakova, M. Pantelev, E. Shnol, Blood coagulation and propagation of autowaves in flow, *Pathophysiol Haemost Thromb* 34 (2005) 135–142. doi:10.1159/000089933.
- [8] R. FitzHugh, Impulses and physiological states in theoretical models of nerve membrane, *Biophysical Journal* 1 (6) (1961) 445 – 466. doi:10.1016/S0006-3495(61)86902-6.
- [9] J. Nagumo, S. Arimoto, S. Yoshizawa, An Active Pulse Transmission Line Simulating Nerve Axon, *Proceedings of the IRE* 50 (10) (1962) 2061–2070. doi:10.1109/jrproc.1962.288235.
- [10] B. Riviere, *Discontinuous Galerkin Methods for Solving Elliptic and Parabolic Equations: Theory and Implementation*, SIAM, 2008.
- [11] T. Akman, B. Karasözen, Variational time discretization methods for optimal control problems governed by diffusion-convection-reaction equations, *Journal of Computational and Applied Mathematics* 272 (2014) 41 – 56. doi:10.1016/j.cam.2014.05.002.
- [12] T. Akman, H. Yücel, B. Karasözen, A priori error analysis of the upwind symmetric interior penalty galerkin (SIPG) method for the optimal control problems governed by unsteady convection diffusion equations, *Computational Optimization and Applications* 57 (3) (2014) 703–729. doi:10.1007/s10589-013-9601-4.
- [13] H. Yücel, B. Karasözen, Adaptive symmetric interior penalty galerkin (SIPG) method for optimal control of convection diffusion equations with

- control constraints, *Optimization* 63 (1) (2014) 145–166. doi:10.1080/02331934.2013.801474.
- [14] H. Yücel, M. Stoll, P. Benner, A discontinuous Galerkin method for optimal control problems governed by a system of convection-diffusion {PDEs} with nonlinear reaction terms, *Computers & Mathematics with Applications* 70 (10) (2015) 2414–2431. doi:10.1016/j.camwa.2015.09.006.
- [15] P. Benner, E. Sachs, S. Volkwein, Model order reduction for pde constrained optimization, in: G. Leugering, P. Benner, S. Engell, A. Griewank, H. Harbrecht, M. Hinze, R. Rannacher, S. Ulbrich (Eds.), *Trends in PDE Constrained Optimization*, Springer International Publishing, Cham, 2014, pp. 303–326. doi:10.1007/978-3-319-05083-6_19.
- [16] M. Gubisch, S. Volkwein, Proper orthogonal decomposition for linear-quadratic optimal control, Tech. rep., University of Konstanz, Department of Mathematics and Statistics, to appear in P. Benner, A. Cohen, M. Ohlberger, and K. Willcox (eds.), *Model Reduction and Approximation: Theory and Algorithms*. SIAM, 2017 (2017).
- [17] W. W. Hager, H. Zhang, Algorithm 851: CG_DESCENT, a conjugate gradient method with guaranteed descent, *ACM Trans. Math. Softw.* 32 (1) (2006) 113–137. doi:10.1145/1132973.1132979.
- [18] M. Hinze, S. Volkwein, Error estimates for abstract linear-quadratic optimal control problems using proper orthogonal decomposition, *Computational Optimization and Applications* 39 (3) (2008) 319–345. doi:10.1007/s10589-007-9058-4.
- [19] K. Kunisch, S. Volkwein, Proper orthogonal decomposition for optimality systems, *ESAIM: Mathematical Modelling and Numerical Analysis* 42 (1) (2008) 1–23. doi:10.1051/m2an:2007054.
- [20] F. Tröltzsch, S. Volkwein, POD a-posteriori error estimates for linear-quadratic optimal control problems, *Computational Optimization and Applications* 44 (1) (2008) 83–115. doi:10.1007/s10589-008-9224-3.
- [21] E. Kammann, F. Tröltzsch, S. Volkwein, A posteriori error estimation for semilinear parabolic optimal control problems with application to model reduction by POD, *ESAIM: Mathematical Modelling and Numerical Analysis* 47 (2013) 555–581. doi:10.1051/m2an/2012037.

- [22] A. Studinger, S. Volkwein, Numerical analysis of POD a-posteriori error estimation for optimal control, in: K. Bredies, C. Clason, K. Kunisch, G. von Winckel (Eds.), *Control and Optimization with PDE Constraints*, Springer Basel, Basel, 2013, pp. 137–158. doi:10.1007/978-3-0348-0631-2_8.
- [23] K. Kunisch, M. Müller, Uniform convergence of the POD method and applications to optimal control, *Discrete and Continuous Dynamical Systems* 35 (9) (2015) 4477–4501. doi:10.3934/dcds.2015.35.4477.
- [24] M. Barrault, Y. Maday, N. C. Nguyen, A. T. Patera, An empirical interpolation method: application to efficient reduced-basis discretization of partial differential equations, *Comptes Rendus Mathématique* 339 (9) (2004) 667–672. doi:10.1016/j.crma.2004.08.006.
- [25] S. Chaturantabut, D. C. Sorensen, Nonlinear model reduction via discrete empirical interpolation, *SIAM Journal on Scientific Computing* 32 (5) (2010) 2737–2764. doi:10.1137/090766498.
- [26] A. Alla, J. N. Kutz, Nonlinear model order reduction via dynamic mode decomposition, arXiv:1602.05080 to appear in *SIAM Journal on Scientific Computing*.
- [27] P. J. Schmid, Dynamic mode decomposition of numerical and experimental data, *Journal of Fluid Mechanics* 656 (2010) 5–28. doi:10.1017/S0022112010001217.
- [28] C. W. Rowley, I. Mezić, S. Bagheri, P. Schlatter, D. S. Henningson, Spectral analysis of nonlinear flows, *Journal of Fluid Mechanics* 641 (2009) 115–127. doi:10.1017/S0022112009992059.
- [29] B. O. Koopman, Hamiltonian systems and transformation in Hilbert space, *Proceedings of the National Academy of Sciences* 17 (5) (1931) 315–318.
- [30] J. N. Kutz, S. L. Brunton, B. W. Brunton, J. L. Proctor, *Dynamic Mode Decomposition: Data-Driven Modeling of Complex Systems*, SIAM, 2016.
- [31] M. Müller, Uniform convergence of the POD method and applications to optimal control, Ph.D. thesis, Karl-Franzens-Universität Graz (2011).
- [32] B. Karasözen, T. Küçükseyhan, M. Uzunca, Structure preserving integration and model order reduction of skew-gradient reaction-diffusion

- systems, *Annals of Operations Research* (2015) 1–28doi:10.1007/s10479-015-2063-6.
- [33] C. Vilas, M. R. Garca, J. R. Banga, A. A. Alonso, Robust feed-back control of travelling waves in a class of reaction-diffusion distributed biological systems, *Physica D: Nonlinear Phenomena* 237 (18) (2008) 2353 – 2364. doi:10.1016/j.physd.2008.02.019.
- [34] A. Lobanov, T. Starozhilova, The effect of convective flows on blood coagulation processes, *Pathophysiol Haemost Thromb* 34 (2005) 121–134. doi:10.1159/000089932.
- [35] F. I. Ataulkhanov, V. I. Zarnitsina, A. V. Pokhilko, A. I. Lobanov, O. L. Morozova, Spatio-temporal dynamics of blood coagulation and pattern formation: A theoretical approach, *International Journal of Bifurcation and Chaos* 12 (09) (2002) 1985–2002. doi:10.1142/S0218127402005649.
- [36] F. Tröltzsch, Optimal control of partial differential equations, Vol. 112 of Graduate Studies in Mathematics, American Mathematical Society, Providence, RI, 2010. doi:10.1090/gsm/112.
- [37] C. Ryll, F. Tröltzsch, Proper orthogonal decomposition in sparse optimal control of some reaction diffusion equations using model predictive control, *PAMM* 14 (1) (2014) 883–884. doi:10.1002/pamm.201410422.
- [38] K. Kunisch, S. Volkwein, Galerkin proper orthogonal decomposition methods for parabolic problems, *Numerische Mathematik* 90 (1) (2001) 117–148. doi:10.1007/s002110100282.
- [39] J. H. Tu, C. W. Rowley, D. M. Luchtenburg, S. L. Brunton, J. N. Kutz, On dynamic mode decomposition: theory and applications, *J. Comput. Dyn.* 1 (2) (2014) 391–421. doi:10.3934/jcd.2014.1.391.
- [40] M. Uzunca, T. Küçükseyhan, H. Yücel, B. Karasözen, Optimal Control of Convective FitzHugh-Nagumo Equation, arXiv e-prints: to appear in *Computers and Mathematics with Applications* (2017).